Dynamics of $O^{8+}+H$ electron capture in Debye plasmas

L. Liu,[1] J. G. Wang,[1] and R. K. Janev[2]
[1]*Institute of Applied Physics and Computational Mathematics, P.O. Box 8009, Beijing 100088, People's Republic of China*
[2]*Macedonian Academy of Sciences and Arts, P.O. Box 428, 1000 Skopje, Macedonia*
(Received 12 November 2008; revised manuscript received 2 April 2009; published 11 May 2009)

The electron capture in $O^{8+}-H$ collisions is studied by the two-center atomic-orbital close-coupling method when the interactions of charged particles are screened and have a Yukawa form. Atomic orbitals and eigenenergies of $n \leq 7$ states on O^{7+} and $n \leq 2$ states on H are calculated as a function of the interaction screening parameter and used in the atomic-orbital close-coupling dynamics scheme to calculate the electron capture cross sections in the energy range of 0.2–50 keV/u. It is shown that the degree of interaction screening determines the reduction in electron binding energies, the number of open electron capture channels, and the strength of the exchange couplings, thus affecting the entire collision dynamics and the magnitude and energy behavior of state-selective cross sections. The changes in electron binding energies and capture cross sections when the interaction screening varies introduce dramatic changes in the radiation spectrum of $O^{7+}(nl)$ capture states with respect to the unscreened interaction case. The state-selective electron capture cross sections in this collision system, as well as the intensities of a number of charge exchange spectral lines, for a number of representative screening parameter values are presented and discussed.

DOI: 10.1103/PhysRevA.79.052702 PACS number(s): 34.20.Cf, 34.70.+e, 52.20.Hv

I. INTRODUCTION

Electron capture processes in collisions between fully stripped ions and atomic hydrogen have been subject to considerable scientific interest for many years in view of their important role in the energy balance and diagnostics of fusion and astrophysical plasmas [1–3]. At the same time, these collision systems with only one electron and two heavy nuclei have served as a testing ground for the theoretical models of the electron capture process with Coulomb interparticle interactions. The significant amount of theoretical and experimental studies of these processes has been reviewed in many articles and books (see, e.g., [4–6]). However, in the environments of hot dense plasmas, where the Coulomb interactions between charged particles may be significantly screened, the atomic collision processes have been investigated relatively scarcely. The results of these studies are reviewed in [7–10].

The electron capture process in proton-hydrogenlike ion collisions in a Debye plasma has been studied in Ref. [11] in the framework of the Bohr-Lindhard classical model [12], but using its high-energy part only. The electron capture and ionization processes in hydrogen atom–fully stripped ion collisions with Debye-Hückel interparticle interactions have been studied in Ref. [13] by using the classical trajectory Monte Carlo method, in which the microcanonical distribution of initial electron coordinates and momenta was determined from the H(1*s*) electron energies in a Debye-Hückel potential. Quite recently, we have performed extensive studies of the excitation and electron capture processes in $H^+ + H(1s)$ [14] and $He^{2+} + H(1s)$ [15] collision systems, as well as for ionization in the latter collision system [16], in a Debye plasma by employing the two-center atomic-orbital close-coupling (TC-AOCC) method with a large expansion basis.

In the present work, we shall study the electron capture process

$$O^{8+} + H(1s) \rightarrow O^{7+}(nl) + H^+ \tag{1}$$

when the electron-ion interaction is described by the Debye-Hückel potential (e is the unit charge),

$$V(r) = -\frac{Ze^2}{r} e^{-r/r_d}. \tag{2}$$

The Debye screening length, r_d, is related to the plasma electron temperature (T_e) and density (n_e) by $r_d = (k_B T_e / 4\pi e^2 n_e)^{1/2}$, where k_B is the Boltzmann constant. Potential (2) is a good representation of the effective two-body electron-ion interaction as long as the Coulomb coupling parameter $\Gamma = e^2/(ak_B T_e)$ and plasma nonideality parameter $\gamma = e^2/(r_d k_B T_e)$ satisfy the conditions $\Gamma \leq 1$, $\gamma \ll 1$, where $a = [3/(4\pi n_e)]^{1/3}$ is the average interparticle distance. There is a wide class of laboratory and astrophysical plasmas in which these conditions are fulfilled (Debye plasmas). In particular, the inertial confinement fusion plasmas with parameters $T_e \sim 0.5-10$ keV and $n_e \sim (0.5-10) \times 10^{24}$ cm^{-3} belong to this type of plasmas.

In our study of process (1) we shall employ the TC-AOCC method, used also in our previous work on ion-atom inelastic processes in Debye plasmas [14–16]. Since the electron capture in the $O^{8+}+H$ collision system populates dominantly the O^{7+} states with high principal quantum number n (around $n \sim 5,6$) [4], the use of a close-coupling method for description of its dynamics requires, generally, a very large expansion basis of atomic (at medium to high collision energies) or molecular (at low collision energies) orbitals. The state selectivity of electron capture process becomes increasingly more pronounced with decreasing the collision energy (see, e.g., [4,5]) and the requirements on the expansion basis can be significantly relaxed. For this reason we choose to study reaction (1) in the energy range of 0.2–50 keV/u in which, at the same time, the use of semiclassical AOCC method is fully applicable [5], although its extension below ~10 keV/u (so-called "molecular region") still re-

quires an adequately large atomic-orbital basis [17,18].

One of the motivations to study process (1) is to investigate the effects of high nuclear-charge asymmetry of the collision system on the electron capture dynamics under the conditions of interaction screening. As we shall see in Sec. III B, this effect is quite remarkable and manifests itself in the increase in cross sections for capture to low-n states ($n=3,4$) when the screening length decreases. Another remarkable feature of this strongly charge-asymmetric system is that some of the partial nl cross sections with screened Coulomb interaction at the energies below ~ 3 keV/u become larger than those in the unscreened case. These phenomena have not been observed in the previously studied $He^{2+}+H$ system [15].

In the plasma free case, electron capture process (1) has been subject to many theoretical studies using various methods to describe its dynamics. Large-scale semiclassical close-coupling cross section calculations have been performed by using AO [18], molecular orbital (MO) [19–21], and hyperspherical (HS) function [22] expansions in the energy region below 30 keV/u. In Refs. [19,20] the expansion basis contained MOs correlating to the H($1s$) state and to the states in the nth manifold of O^{7+}, where $n=4,5,6$, as well as some states from the neighboring manifold (e.g., from $n=7$ in Ref. [19]). Therefore, neither the intramanifold nor the intermanifold state coupling in the group of $n=4,5,6$ manifolds was completely accounted for in the calculations in Refs. [19–21] (resulting in the use of 33 [19] and 30 [20] MOs in the expansion basis). The HS close-coupling calculations in Ref. [22] used a basis of 33 hyperspherical functions, while the AOCC calculations in Ref. [18] used a basis containing all AOs from the $n=4,5,6$ manifolds (a total of 46 AOs). As the cross-section calculations in the present work are extended to 50 keV/u, we include in the AO basis all the O^{7+} states with $n\leq 7$ (in total 84) and the $1s$, $2s$, and $2p_{0,1}$ states of H.

The paper is organized as follows. In Sec. II we briefly outline the theoretical method used in the cross section calculations. In Sec. III, we present the results of cross sectional calculations for process (1) for different values of the screening length r_d and analyze the effects of the screening on the dynamics of the process. As an application of the calculated state-selective electron capture cross sections, we present in Sec. IV the results of the calculations of intensities of a number of spectral lines emitted from the charge exchange populated O^{7+} excited states and analyze the effect of the interaction screening on their intensity and frequency. In Sec. V, we give our conclusions.

Atomic units will be used in the remaining part of this paper unless explicitly indicated otherwise.

II. THEORETICAL CONSIDERATIONS

A. Wave functions and energies of bound states in a Debye-Hückel potential

The application of TC-AOCC method to an ion-atom collision system requires determination of single-center electronic states over which the total scattering wave function is expanded and used in time-dependent Schrödinger equation to generate the coupled equations for the state amplitudes.

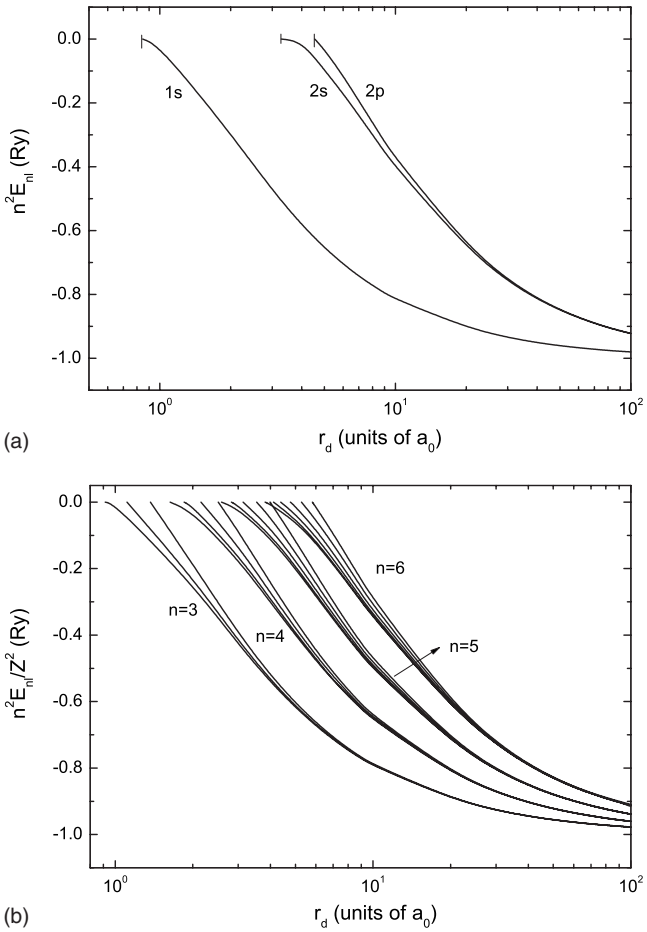

FIG. 1. (a) r_d dependence of energies of (a) $1s$ and $2l$ states of H and (b) of $3l$, $4l$, $5l$, and $6l$ states of O^{7+}.

For determining the bound electronic states with potential (2) on either of the two centers, we have used the variational method with even-tempered trial functions [23,24],

$$\chi_{klm}(\vec{r};r_d) = N_l(\xi_k(r_d))r^l e^{-\xi_k(r_d)r}Y_{lm}(\hat{\vec{r}}),$$

$$\xi_k(r_d) = \alpha\beta^k, \quad k=1,2,\ldots,N, \tag{3}$$

where $N_l(\xi_k)$ is a normalization constant, $Y_{lm}(\boldsymbol{r})$ are the spherical harmonics, and α and β are variational parameters, determined by minimization of the energy for each value of r_d. The atomic states $\phi_{nlm}(\vec{r};r_d)$ are then obtained as linear combination

$$\phi_{nlm}(\vec{r};r_d) = \sum_k c_{nk}\chi_{klm}(\vec{r};r_d), \tag{4}$$

where the coefficients c_{nk} are determined by diagonalization of single-center Hamiltonian. This diagonalization yields the energies $E_{nl}(r_d)$ of the bound states in the screened Coulomb potential.

The r_d dependences of energies of $1s$ and $2l$ states of H and of $3l$, $4l$, $5l$, and $6l$ states of O^{7+} are shown in the panels (a) and (b) of Fig. 1, respectively. It is evident from this figure that in potential (2) the Coulomb degeneracy of l substates within a given n manifold is lifted and that with de-

TABLE I. Critical screening lengths, $r_{d,c}^{nl}$ (a_0), for $n \leq 2$ states of H and $n \leq 7$ states of O^{7+}.

H	n/l	0	1	2	3	4	5
	1	0.8450					
	2	3.2800	4.5420				
O^{7+}	n/l	0	1	2	3	4	5
	1	0.1056					
	2	0.4079	0.56765				
	3	0.9146	1.1101	1.36845			
	4	1.6350	1.8512	2.1521	2.5085		
	5	2.5860	2.8210	3.1360	3.5339	3.9888	
	6	3.8110	4.1080	4.3876	4.7760	5.2790	5.8143
	7	5.3660	5.956	6.1505	6.4070	7.5082	7.8513

creasing r_d the energy of atomic states decreases and eventually enters the continuum at certain critical Debye length, $r_{d,c}^{nl}$. This implies that potential (2) supports only a finite number of nondegenerate states for any finite value of r_d, a well known property of any potential that decreases faster than $-1/r^2$ when r tends to infinity (see, e.g., [25]). From the point of view of collision dynamics of processes involving the discrete spectrum of colliding particles, the critical Debye length for an nl state is of obvious relevance. In Table I we give the values of $r_{d,c}^{nl}$ for the $1s$ and $2l$ states of H and of the all $n \leq 7$ states of O^{7+}.

From Fig. 1 it can also be seen that the energy difference $\Delta E_{n+1,l\pm k;nl} = E_{n+1,l\pm k}, -E_{nl} (k=0,1,2,\ldots)$ decreases with decreasing r_d, particularly for $\Delta E_{n+1,l-k;nl}$. In Fig. 2 we show the energy differences $\Delta E_{np;1s}$ for $n \leq 5$ states of O^{7+} ion when r_d varies in a more explicit way. The reduction in energy difference between these considered states is particularly pronounced when the energy of the upper state approaches the value of its critical Debye length. Obviously, the variation in both E_{nl} and $\Delta E_{n+1,l-k;nl}$ with varying the screening length r_d has important spectroscopic consequences.

From the point of view of collision dynamics the energy difference between the initial and final capture states is also important, $\Delta E_{nl(O7+);1s(H)}$. In Fig. 3 we show this difference for the $nl=3d$, $4f$, $5g$, and $6h$ states of O^{7+} as a function of screening length r_d. It should be noted that the energy differences $\Delta E_{nl(O7+);1s(H)}$ start to decrease with decreasing r_d already at its large values and that at certain values of $r_{d,0}^{nl}$ they change sign, $\Delta E_{nl(O7+);1s(H)}(r_{d,0}^{nl}) = 0$. For these values of r_d the initial and final states in reaction (1) are in energy resonance.

B. Coupled channel equations and electron exchange couplings

In the collision energy range considered in the present paper (0.2–50 keV/amu), the straight-line approximation for the relative nuclear motion, $R(t) = \vec{b} + \vec{v}t$ (b is the impact parameter and v is the collision velocity) can be safely adopted, as discussed in Sec. I (see also [5]). The TC-AOCC equations are then obtained by expanding the total electron wave function Ψ in terms of atomic orbitals of both centers multiplied by plane wave electron translational factors [17]

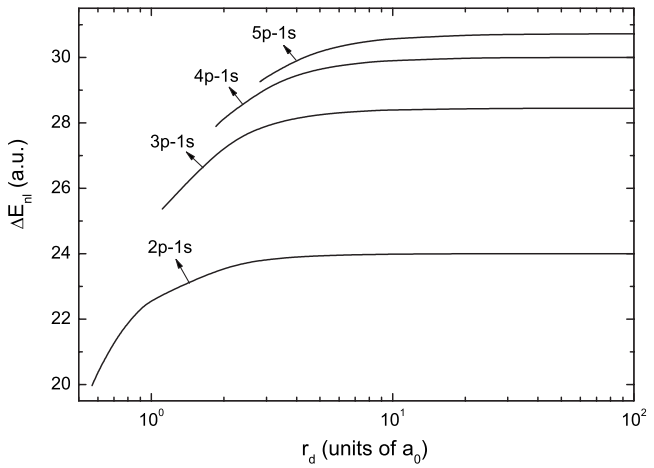

FIG. 2. r_d dependence of the energy difference $\Delta E_{np;1s}$ for $n \leq 5$ states of O^{7+} in the region $r_d \leq 100a_0$.

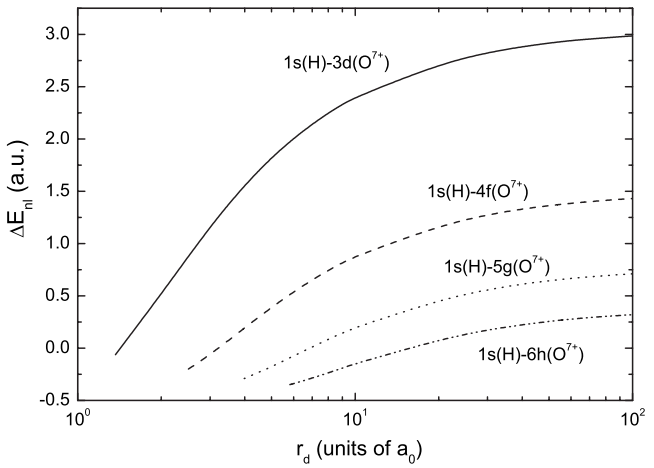

FIG. 3. r_d dependence of the energy difference $\Delta E_{nl(O7+);1s(H)}$ in the region $r_d \leq 100a_0$.

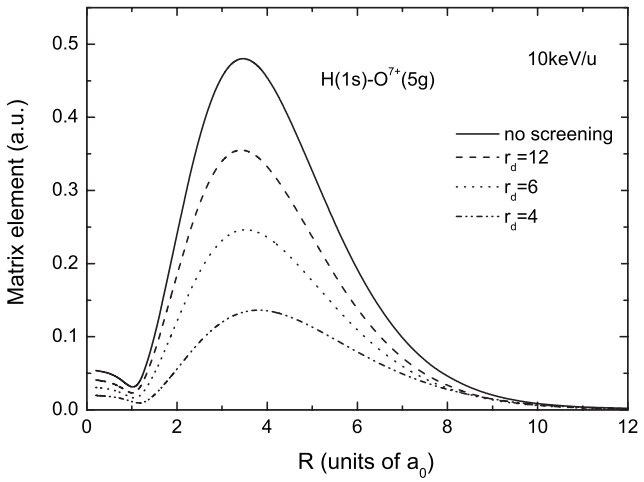

FIG. 4. Variation in absolute values of matrix element for $H(1s) \rightarrow O^{7+}(5g)$ electron exchange transition for a number of r_d values and for the unscreened case.

$$\Psi(\vec{r},t;r_d) = \sum_i a_i(t)\phi_i^A(\vec{r};t;r_d) + \sum_j b_j(t)\phi_j^B(\vec{r};t;r_d) \quad (5)$$

and inserting it in the time-dependent Schrödinger equation $(H - i\frac{\partial}{\partial t})\Psi = 0$, where $H = -\frac{1}{2}\nabla_r^2 + V_A(r_A) + V_B(r_B)$ and $V_{A,B}(r_{A,B})$ are the electron interactions of form (2) with the target nucleus (H^+) and the projectile (O^{8+}), respectively. The resulting first-order coupled equations for the amplitude $a_i(t)$ and $b_j(t)$ are

$$i(\dot{A} + S\dot{B}) = HA + KB, \quad (6a)$$

$$i(\dot{B} + S^{\dagger}\dot{A}) = \bar{K}A + \bar{H}B, \quad (6b)$$

where A and B are the vectors of the amplitudes $a_i (i = 1,2,\ldots,N_A)$ and $b_j (j = 1,2,\ldots,N_B)$, respectively. S is the overlap matrix ($S^{\dagger}$ is its transposed form), H and $\bar{H}$ are direct coupling matrices involving the states in H and O^{7+}, respectively, and K and $\bar{K}$ are the electron exchange matrices. The system of Eq. (6) is to be solved under the initial conditions

$$a_i(-\infty) = \delta_{1i}, \quad b_j(-\infty) = 0. \quad (7)$$

After solving the system of coupled Eq. (6), the cross section for $1 \rightarrow j$ electron capture transition is calculated as

$$\sigma_{cx,j} = 2\pi \int_0^{\infty} |b_j(+\infty)|^2 b db. \quad (8)$$

The sum of $\sigma_{cx,j}$ over j gives the corresponding total electron capture cross section.

An insight into the dynamics of electron capture process (1) in a Debye plasma can be obtained by analyzing the variation with r_d of electron exchange matrix elements $K_{1s,nl}$ for different collision energies. As an example of the behavior of these matrix elements we show in Fig. 4 the absolute values of $K_{1s,5g}$ for the zero-screening case and for the screening cases with $r_d = 12a_0$, $6a_0$, $4a_0$, and $2.5a_0$ for the collision energy of 10 keV/u. We observe a significant reduction in the values of the matrix elements with decreasing r_d. Similar behaviors with varying r_d show also the other exchange coupling elements, as well as those for direct coupling of the states on the same center. We also note that for a given n and r_d the exchange matrix elements increase with increasing l.

III. CROSS SECTION RESULTS

A. Unscreened Coulomb interaction: Test of the basis sufficiency

As mentioned in Sec. I, in solving the coupled channel [Eq. (6)] we have used in expansion (5) all the $n \leq 7$ states of O^{7+} and the $n \leq 2$ states of H, a total of 84 states. In the considered energy range (0.2–50 keV/u), however, the $O^{7+}(n \leq 2)$ and $H(n=2)$ states should not play any considerable role in the collision dynamics. We would like first to check the sufficiency of adopted basis from the point of view of reliability of calculated cross sections for the case of unscreened Coulomb interaction for which, as mentioned earlier, other extensive cross section calculations for this reaction already exist.

The results of our total and n-selective electron capture cross sections for the zero-screening case are shown in Figs. 5(a) and 5(b), respectively. They are compared with the results of previous large-scale coupled channel calculations using the AOCC method [18] (with 47 AOs in the basis), the MOCC method [19–21] (with 33 MOs [19] and 30 MOs [20] in the basis), and the HSCC method [22] (with 33 hyperspherical functions in the basis). In Fig. 5(a) the total experimental cross section in Ref. [26] is also shown. The total cross section of present calculations agrees well with the 33-HSCC [21] and MOCC [19] calculations in the entire overlapping energy region, as well as with the AOCC [18] and MOCC [20,21] total cross sections and experimental data at energies above ~1 keV/u. In the region below this energy, the total AOCC [18] and MOCC [20] cross sections are smaller than those of the present calculations and in Refs. [19,22] but appear to be closer to the experimental data. The discrepancy of the HSCC and MOCC [19] cross sections with those in Refs. [18,20] was analyzed in detail in Ref. [22] and was ascribed to the use in Ref. [18] of curved (Coulomb) trajectories for the nuclear motion in the exit channels of reaction (1), while the disagreement with the MOCC results in Ref. [20] remains still unclear. An insight in this disagreement can be gained from Fig. 5(b), where the n-partial cross sections from the present and previous calculations are displayed. In the present calculations, as well as in those in Refs. [19,22], the dominant electron capture channels for E smaller than ~1 keV/u are the $n=5$ and $n=6$ channels, while in Refs. [18,20] that is only the $n=5$ channel. In fact, in the energy region bellow ~100 keV/u, the $n=6$ channel becomes dominant in the calculations in Refs. [19,22]. The calculations in Ref. [27] performed for this system with the advanced adiabatic (or hidden crossing) method also predict dominant population of $n=5$ and $n=6$ capture channels in the region below ~1 keV/u, with the $n=6$ becoming the dominant one below ~200 eV/u. (The data in Ref. [27], however, are significantly below those in Refs. [19,22] and are not shown in Figs. 5(a) and 5(b).) We further

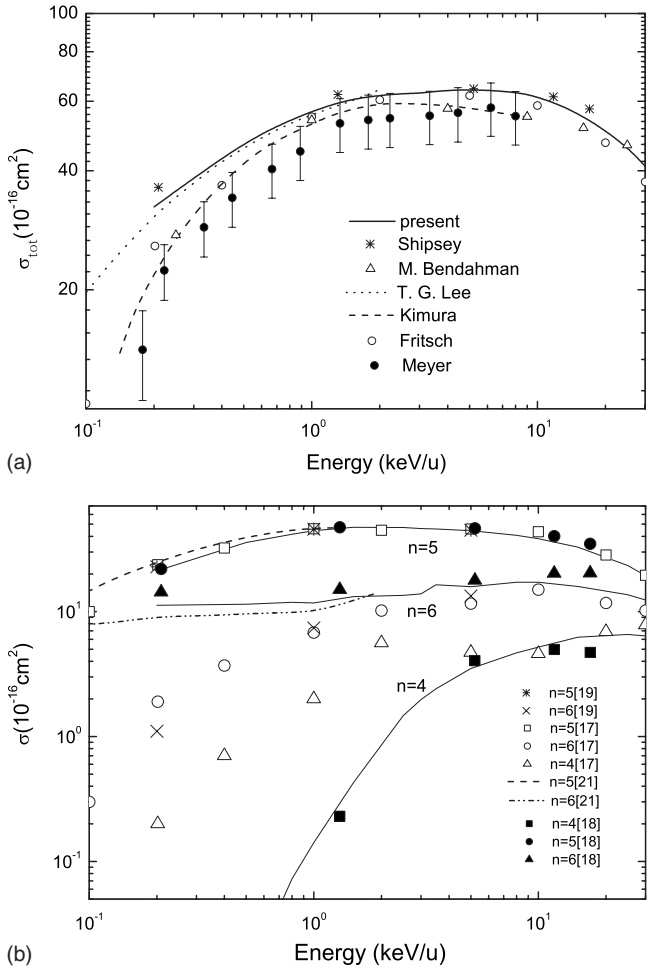

FIG. 5. (a) The total charge transfer cross sections for O^{8+}+H($1s$) collision as functions of collision energy. Theoretical results: (—) present results and (– – –) the results of Kimura, (• • •) Lee *et al.*, (***) Shipsey *et al.*, (○) Fritsch and Lin, and (△) Bendahman *et al.*; experimental results: (●) Meyer *et al.* (b) Partial charge transfer cross sections for $O^{7+}(nl)$, $n=4,5,6$.

mention that in Ref. [22] 47 AOCC calculations were also performed with straight-line trajectories for the nuclear motion producing results for capture to $n=5$ and $n=6$ shells of O^{7+} close to those of the HSCC calculations. All this indicates that with the AO basis adopted in the present work, our TC-AOCC cross section calculations can be considered reliable in the 0.2–50 keV/u energy range. We should note in Fig. 5(b) that the cross section for capture to the $n=7$ shell of O^{7+} is comparable with those for $n=4,5,6$ at energies above 20–30 keV/u.

Since the main goal of the present paper is the study of electron capture dynamics with screened Coulomb interactions of Yukawa type, we need a convergence check of the results obtained by the adopted AO basis in the case of screened interactions. In Table II we compare the total cross sections for the collision energy of 10 keV/u calculated with basis sets containing all $n\leq 2$ states on H^+ and all states with $n\leq 6$, $n\leq 7$, and $n\leq 8$ centered on O^{7+} for $r_d=\infty$, $12a_0$, $6a_0$, and $2.5a_0$. We see that with the basis set containing all $n\leq 7$ states on O^{7+} the convergence of the results can be considered as being achieved for this energy for all considered values of the Debye length (to within 0.1–0.3%), including also the unscreened case. We have performed a convergence check also for the energy of 50 keV/u and found that the results for the total cross sections with the $n\leq 7$ basis are convergent to within 10%.

TABLE II. Total electron capture cross sections in 10 keV/u O^{8+}+H collisions for the unscreened case ($r_d=\infty$) and for the screened cases with $r_d=12a_0$, $6a_0$, and $2.5a_0$, calculated with basis sets containing all states with $n\leq 6$, $n\leq 7$, and $n\leq 8$ of O^{7+}.

E (keV/u)	$r_d(a_0)$	$n\leq 6$	$n\leq 7$	$n\leq 8$
10	Infinity	60.36669	61.61491	61.83155
	12	54.04910	54.72293	54.67007
	6	42.02205	42.52779	42.44357
	2.5	17.67540	16.30848	16.25306

B. Capture cross sections with screened Coulomb interaction

Now we turn to the investigation of the effects of interaction screening on the electron capture dynamics and cross sections. The most significant effect of the interaction screening on the electron capture dynamics is the shift of discrete energy levels with decreasing in the Debye length and entering the continuum at the critical values $r_{d,c}^{nl}$, as discussed in Sec. III A. This limits the open electron capture channels to a finite number for a given finite value of the screening length. The decrease in electron exchange matrix elements with decreasing Debye length (see Fig. 4) also leads to a decrease in the magnitude of the cross sections of the available electron capture channels for a given value of r_d. At low energies (below ~3–5 keV/u), the decrease in energy difference between the initial and final states, $\Delta E_{nl(O7+);1s(H)}$ (see Fig. 3) with decreasing r_d, also starts to play an important role in the collision dynamics. In the regions of internuclear distance R where the difference $\Delta E_{nl(O7+);1s(H)}$ becomes small, the zone of strong interaction between the corresponding states, $\Delta R \sim 1/\Delta E_{nl(O7+);1s(H)}$, becomes larger. At low relative collision velocities the system spends longer time in this interaction zone and that leads to increase in transition probability. In a quasimolecular description of collision dynamics (which is more appropriate for this energy region), this would correspond to the nonadiabatic transitions between corresponding molecular states caused by their radial coupling (see, e.g., [4,5]). According to the adiabatic Massey criterion, the transitions between electronic states are strong when the condition $\Delta R H_{12}^2/v \sim 1$ is fulfilled, where H_{12} is the matrix element coupling the interacting states and v is the collision velocity. In a multistate collision system, the coupling between the initial and final states is determined not only by their direct coupling but also by the couplings of intermediate states among themselves and with the initial and final states. The series of two-state strong coupling regions during the time evolution of the system can greatly extend the effective strong coupling region between the initial and final states. This is particularly true under the conditions of lifted

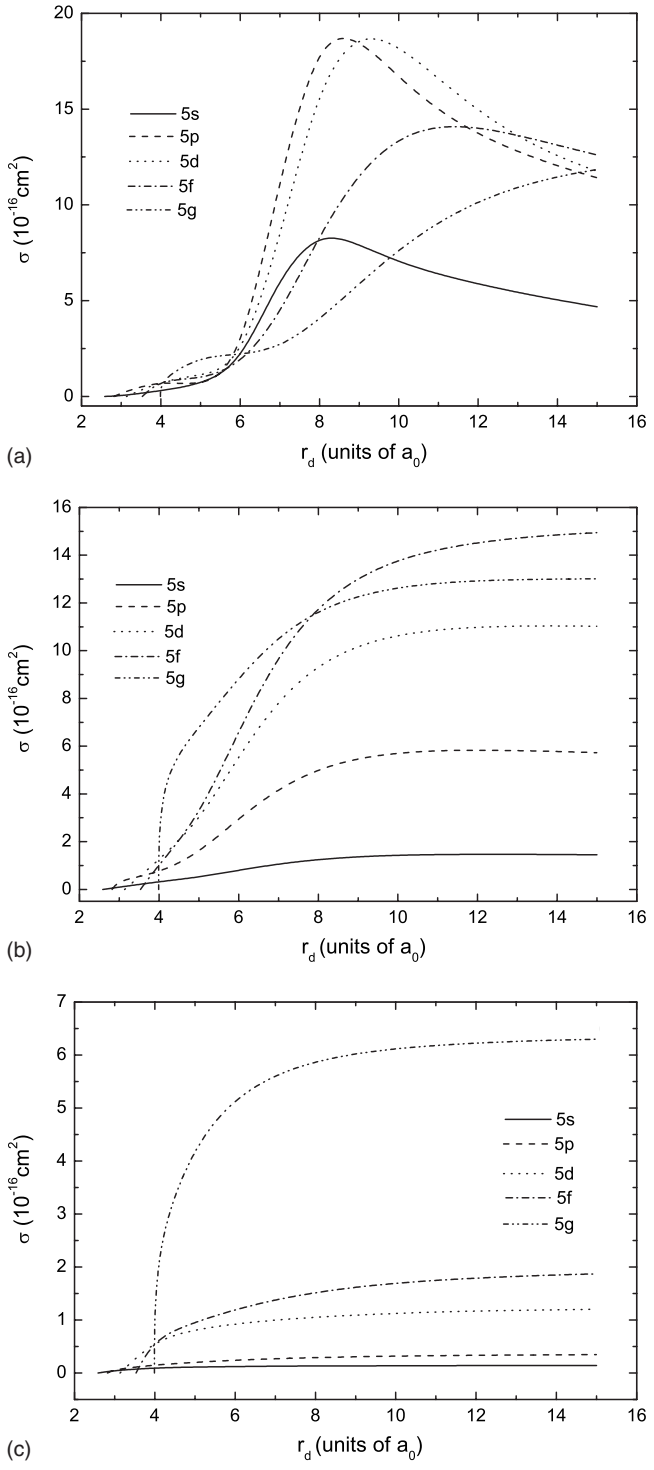

FIG. 6. Cross sections for electron capture to $5l$ states of O^{7+} as a function of screening length for E=0.5 keV/u [panel (a)], E=5 keV/u [panel (b)], and E=50 keV/u [panel (c)].

l degeneracy when the density of two-state strong coupling regions is high.

The complex character of the variation in electron capture collision dynamics when varying the screening length and collision energy is demonstrated in Fig. 6 where the partial cross sections for capture to the $5l$ states as a function of the screening length are shown for the energies of 0.5 [panel (a)], 5 [panel (b)], and 50 [panel (c)] keV/u. Each of these cross sections tends to zero when r_d tends toward the limiting value $r_{d,c}^{nl}$ of the corresponding state. It is interesting to note in Fig. 6(a) that, except for the $5g$ state, the cross sections for all $5l$ states for r_d above certain value are larger than their values in the screening-free case. This is an effect of the reduced energy difference between the initial and final states and of the extended coupling time at this energy, as discussed above. It is also interesting to note that the cross sections for capture to $5p$ and $5d$ states are the largest ones up to r_d about $(12-13)a_0$. The role of these states in the capture dynamics, however, changes with increasing the energy when the population of high-l starts to dominate [see Figs. 5(b) and 5(c)], with that for the $5g$ state becoming the predominant one for 50 keV/u. This behavior of partial cross sections with varying r_d is, more or less, typical for the other nl capture channels as well. In general, the partial cross sections decrease with decreasing the screening length when the collision energy is larger than ~5 keV/u.

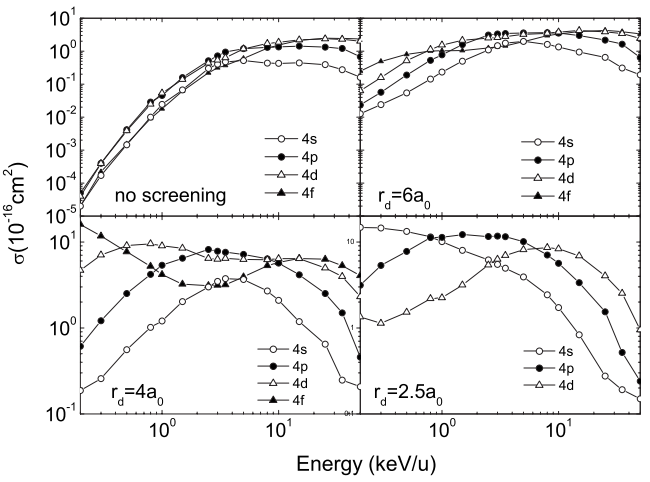

FIG. 7. Energy dependence of state-selective cross sections for electron capture to $4l$ states of O^{7+} for the no screening case and screening cases with r_d=6a_0, 4a_0, and 2.5a_0. The symbols are open circles for $4s$, filled circles for $4p$, open triangles for $4d$, and filled triangles for $4f$. The lines connecting the calculated points are guides for the eyes.

We shall now investigate in more detail the energy behavior of partial cross sections for specific values of the Debye length. In order to illustrate the effects of the screening on the electron capture dynamics in the O^{8+}+H system, we choose the screening lengths r_d=12a_0, 6a_0, 4a_0, and 2.5a_0 since the critical screening lengths $r_{d,c}^{nl}$ for the most important capture states lie in the range of $(2.5-12)a_0$ (see Table I). For a plasma with density of 10^{24} cm^{-3}, the screening lengths 2.5a_0, 4a_0, 6a_0, and 12a_0 would correspond to plasma temperatures of about 0.3, 0.8, 1.8, and 8 keV, respectively, while for a plasma with temperature of 10 keV, the plasma densities corresponding to the above values of the screening length would be about 2.3×10^{24}, 9×10^{23}, 4×10^{23}, and 1×10^{23} cm^{-3}.

In Fig. 7, we show the $4l$ capture cross sections as a function of energy for the unscreened case [panel (a)] and for screened cases with r_d=6a_0, 4a_0, and 2.5a_0, [panels (b)–(d),

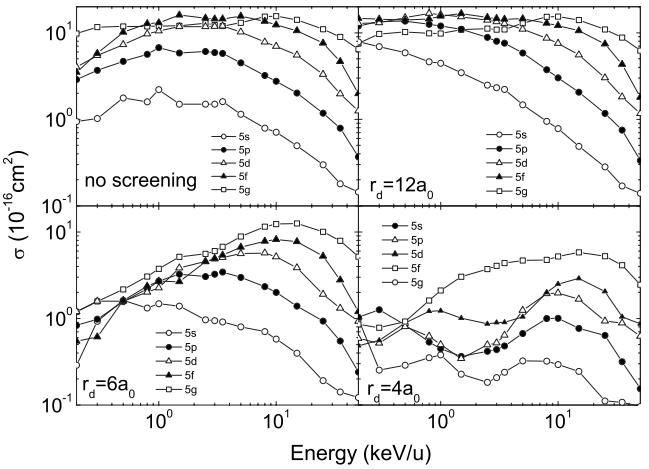

FIG. 8. Energy behavior of state-selective cross sections for electron capture to $5l$ states of O^{7+} for the no screening case and screening cases with $r_d=12a_0$, $6a_0$, and $4a_0$. The symbols are open circles for $5s$, filled circles for $5p$, open triangles for $5d$, filled triangles for $5f$, and open squares for $5g$. The lines connecting the calculated points are guides for the eyes.

respectively]. The $4l$ cross sections for the screened case with $r_d=12a_0$ do not differ much from those in the unscreened case. In Fig. 7(a) we see that the $4l$ cross sections in the zero-screening case rapidly decrease with decreasing the energy below 3–5 keV/u. In the case of interaction screening with $r_d=6a_0$ [Fig. 7(b)], this general behavior is maintained, except for the nonmonotonic decrease in the $4f$ cross section below 2–3 keV/u. The relative increase in this cross section with respect to other $4l$ cross sections in this energy region is associated with the appearance of a strong interaction zone on the internuclear distance due to the decreased energy difference of $O^{7+}(4f)$ and $H(1s)$ states at this value of r_d and the small collision velocity. It should be noted in Fig. 7(b) that all $4l$ partial cross sections are significantly larger than the corresponding ones in the zero-screening case. This is a consequence of both the decrease in energy difference between the states and of the fact that for $r_d=6a_0$ only the $7s$ and $7p$ states of the $n=7$ manifold remain in the discrete spectrum of O^{7+} (see Table I). Since the coupling with the continuum states is much smaller than that between the discrete states, this blocks the capture flux to the reduced number of available capture states and results in increase in their population. This effect is even more pronounced when $r_d=4a_0$ [Fig. 7(c)] in which case the discrete states on O^{7+} are reduced to those with $n\leq 5$ and $6s$ (see Table I). For this value of r_d the condition for strong interaction with the initial state is fulfilled also for the $4d$ state at the energy about 0.8 keV/u, producing a peak in the $4d$ cross section. The $4f$ capture cross section continues to increase with decreasing the energy due to contributions from indirect transitions (series of strong two-state intermediary couplings). Finally, Fig. 7(d) shows the $4s$, $4p$, and $4d$ cross sections for $r_d=2.5a_0$. For this value of r_d the $4f$ state is already in the continuum. It is worthwhile to note that in this case the population of $4d$ state in the low-energy region is not anymore governed by the strong interaction producing the cross section maximum at about 0.8 keV/u and that a series of strong couplings makes

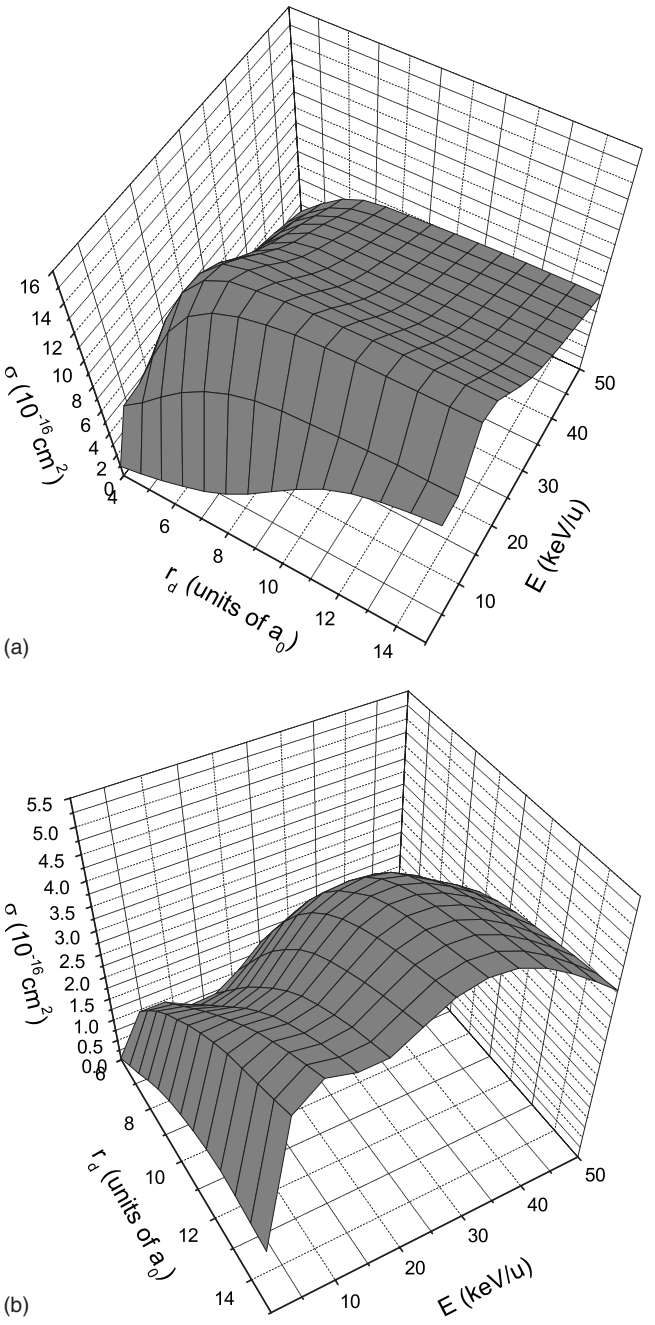

FIG. 9. Dependence on the energy and screening length of the cross sections for electron capture to $5g$ [panel (a)] and $6h$ [panel (b)] states of O^{7+}.

the $4s$ cross section to steadily increase in the region below 2–3 keV/u, in contrast to its energy behavior for larger r_d values. The relative magnitude of the $4l$ capture cross sections above ~25–30 keV/u in all cases presented in Fig. 7 reflects the fact that the exchange coupling matrix elements for a given r_d are larger for the larger l. At these collision energies the indirect couplings (via intermediate states) do not contributes significantly to the cross sections.

We note that the partial $3l$ cross sections for the $r_d=12a_0$, $6a_0$, $4a_0$, and $2.5a_0$ screening lengths show an energy behavior similar to that of $4l$ cross sections.

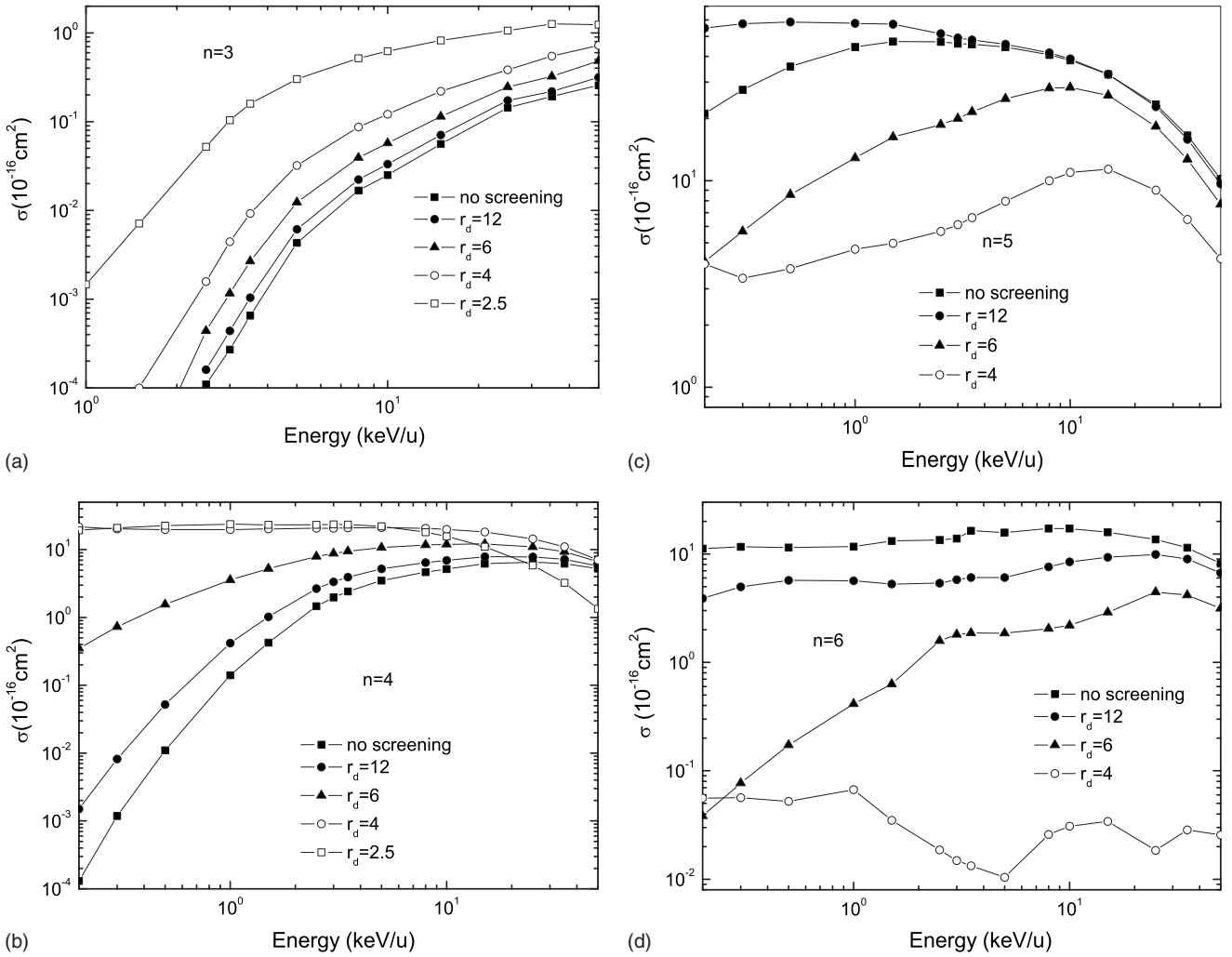

FIG. 10. Energy dependence of partial cross sections for electron capture to $O^{7+}(nl)$, $n=3,4,5,6$ [panels (a)–(d), respectively] for the unscreened case and screened case with $r_d=12a_0$, $6a_0$, $4a_0$, and $2.5a_0$. The symbols are for no screening case (filled squares), $r_d=12a_0$ (filled circles), $r_d=6a_0$ (filled triangles), $r_d=4a_0$ (open circles), and $r_d=2.5a_0$ (open squares).

The energy dependence of $5l$ state-selective cross sections for the unscreened case and for $r_d=12a_0$, $6a_0$, and $4a_0$ are shown in Figs. 8(a)–8(d), respectively. For $r_d=2.5a_0$ all $5l$ states are already in the continuum. As in the case of capture to $4l$ states, the population of individual $5l$ states for energies above ~10 keV/u is larger for the higher l substates. Dominantly populated states in the unscreened case at all energies are $5g$, $5f$, and $5d$ states, whereas in the $r_d=12a_0$ screened case capture to the $5p$ state becomes comparable to the capture to $5g$, $5f$, and $5d$ states for energies below ~3 keV/u due to the capture mechanisms discussed above. It should be noted that the $5l$ capture cross sections are significantly larger than those for the other n manifolds almost in the entire energy range considered. It is also worthwhile to note the decrease in $5l$ cross sections for the $r_d=6a_0$ screened case for energies below ~3 keV/u (except that for $5s$ which starts to decrease only for E below 0.5 keV/u).

The partial $6l$ cross sections for $r_d=12a_0$, $6a_0$, $4a_0$, and $2.5a_0$ have an energy behavior similar to that of $5l$ cross sections.

A more complete picture of the dependences of nl-partial cross sections on both the energy and the screening length is illustrated in Figs. 9(a) and 9(b) for the σ_{5g} and σ_{6h} cross sections, respectively.

In Fig. 10 we show the energy dependence of partial cross sections for capture to $n=3$, 4, 5, and 6 [panels (a)–(d), respectively] for $r_d=12a_0$, $6a_0$, $4a_0$, and $2.5a_0$ and for the unscreened case. The n-partial cross sections for $n=3,4$ and $n=5,6$ in the considered energy range have quite different behavior when r_d varies. With decreasing r_d the cross sections for capture to $n=3$ and $n=4$ increase, whereas those for $n=5$ and $n=6$ decrease, with the exception of $n=5$ cross section for $r_d=12$ which below 10 keV/u is larger than that for zero screening. This behavior of the n-capture cross section is obviously a direct consequence of the different energy behaviors of nl state-selective cross sections when r_d varies, as discussed above for the capture to $4l$ and $5l$ states of O^{7+} (cf. Figs. 7 and 8). The rapid decrease in $n=3$ cross sections in both the unscreened and screened cases with decreasing the energy is "adiabatic" in nature (weak couplings), while their increase with decreasing r_d is a result of the increased transition probability when the energy difference between the states decreases, as discussed earlier. These arguments apply also to the behavior of $n=4$ cross sections [Fig. 10(b)]. The

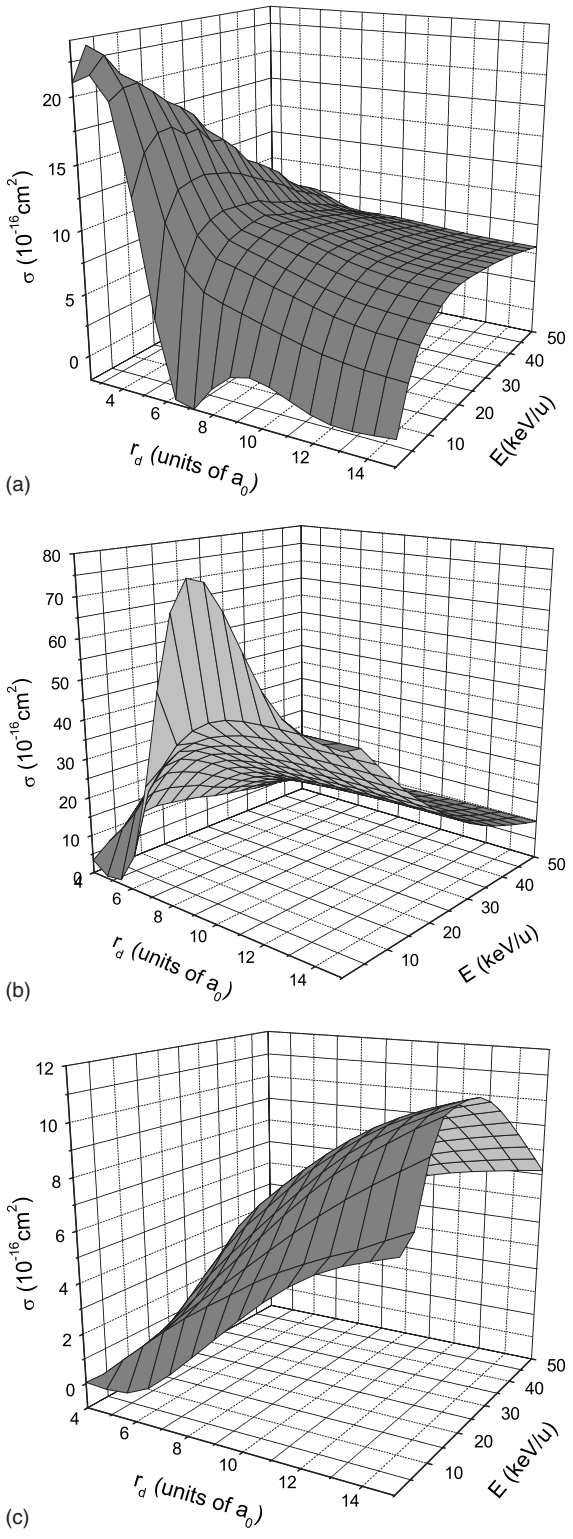

FIG. 11. Dependence on the energy and screening length of the cross sections for electron capture to $n=4$ [panel (a)], $n=5$ [panel (b)], and $n=6$ [panel (c)] shells of O^{7+}.

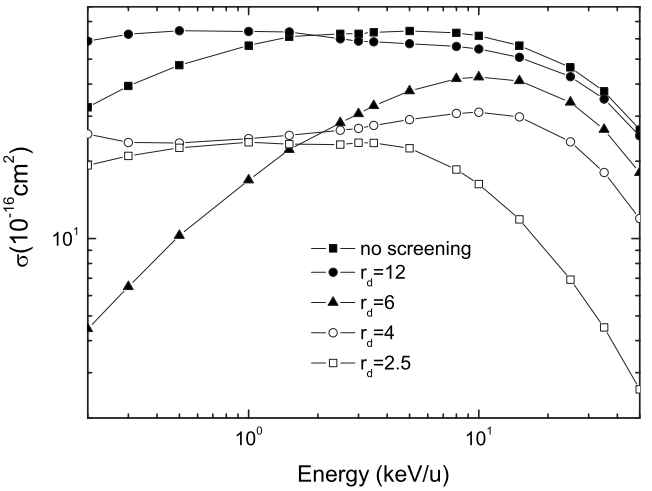

FIG. 12. Total electron capture cross sections for O^{8+}+H collisions with and without screening. The degree of the screening is indicated by the value of r_d. The lines connecting the calculated points are guides for the eyes.

decrease in the $n=4$ cross section for $r_d=2.5a_0$ at energies above 6 keV/u is due to the decrease in exchange coupling matrix elements $1s-4d$, $4p$ with increasing the collision energy for this value of r_d. (As mentioned above, the $4f$ state for $r_d=2.5a_0$ lies already in the continuum.) We note that the difference between the cross sections in the screened and unscreened cases diminishes when the energy approaches 50 keV/u. Additional calculations have shown that at still higher collision energies, the cross sections for $r_d=4a_0$, $6a_0$, and $12a_0$ become smaller than that for the unscreened case, as is the case with the $r_d=2.5a_0$ cross section already for $E \geq 25$ keV/u. This is a result of the predominance of the direct exchange coupling between the initial and final states in determining the cross section at high energies and their decrease with decreasing r_d.

The cross section for capture to $n=5$ in the screening case with $r_d=12a_0$ is significantly larger than that in the unscreened case in the energy region below 2–3 keV/u [see Fig. 10(c)] due to large values of all $5l$ state-selective cross sections in this region [cf. Fig. 8(b)]. However, for $E \geq 25$ keV/u this cross section also becomes smaller than the one for the unscreened case for reasons discussed above. For $r_d=6a_0$ and $r_d=4a_0$ the $n=5$ cross sections are smaller than the one in unscreened case due to the reduction in the number of open capture channels. The reduction in the open reaction channels is also the reason for the smaller values of $n=6$ cross sections with respect to the unscreened case in Fig. 10(d), which is particularly pronounced in the $r_d=4a_0$ case when the $6s$ state is absent in the discrete spectrum of O^{7+}. In the screening case with $r_d=6a_0$ both $n=5$ and $n=6$ cross sections rapidly decrease with decreasing the energy in the region below the cross section maximum. As discussed earlier in connection with Fig. 8(c) for the $n=5$ case, this is a result of the inefficiency of low-energy indirect couplings for this particular value of r_d.

A more complete picture of the energy and r_d dependences of the $n=4$, 5, and 6 partial cross sections can be gained from their three-dimensional (3D) plots in Figs. 11(a)–11(c), respectively.

The energy dependence of the total electron capture cross sections for the unscreened case and for interaction screening with $r_d=12a_0$, $6a_0$, $4a_0$, and $2.5a_0$ are shown in Fig. 12. For energies above 3–5 keV/u, the total cross sections in the

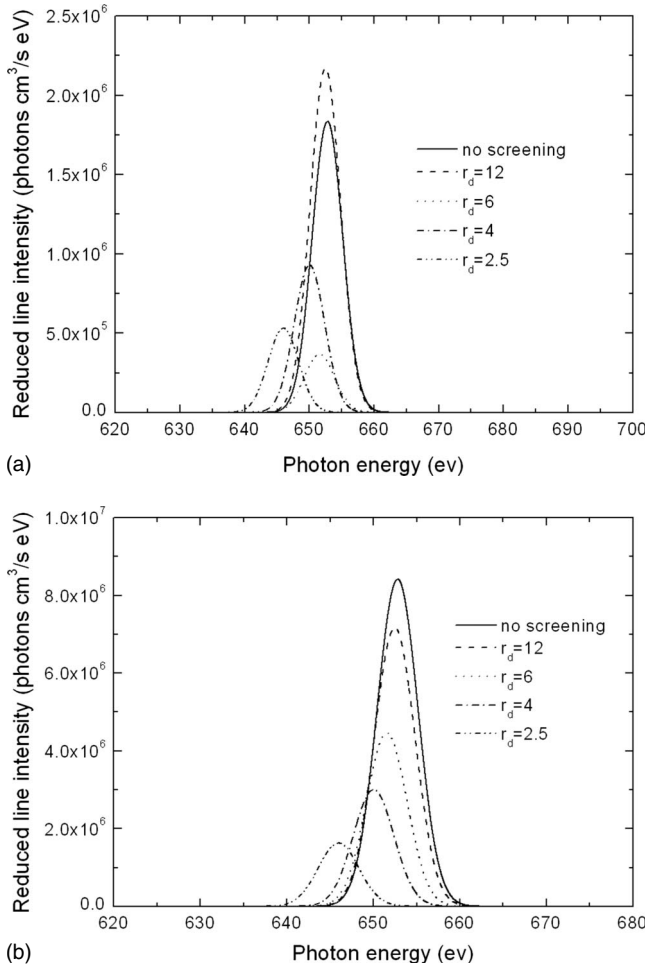

FIG. 13. Reduced intensity of Ly-α line of O^{7+} ion [Eq. (10)], produced by electron capture at collision energies of (a) 0.5 and (b) 5 keV/u for the unscreened and screened cases with $r_d=12a_0$, $6a_0$, $4a_0$, and $2.5a_0$.

screened cases are smaller than the cross section of the unscreened case and their magnitude decreases with decreasing the screening length in accordance with the similar decrease in dominantly populated individual nl cross sections within a given n manifold. In the energy region below ~3 keV/u, the magnitude and energy behavior of total cross sections for $r_d=12a_0$ and $r_d=6a_0$ are determined by the dominant contribution of the $n=5$ cross section, while the cross sections for $r_d=4a_0$ and $r_d=2.5a_0$ are determined by the contribution from the $n=4$ partial cross section. It is interesting to note that while in the unscreened case the $n=6$ cross section becomes comparable with that for $n=5$ in the energy region below ~0.3 keV/u, in the screened case with $r_d=12a_0$ it is about ten times smaller than the $n=5$ cross section.

IV. PROPERTIES OF CHARGE EXCHANGE SPECTRAL LINES

Since the emission from the ion states populated by the electron capture process is an important radiative loss mechanism in hot dense plasmas and since it can serve for diagnostic purposes, it is of considerable interest to investigate the changes in the spectral line properties (intensity, line shift, and broadening) due to the interaction screening by the plasma. In the present section we assume that the population of O^{7+} excited states is determined exclusively by the electron capture from H(1s). The number of the emitted photons per second and cm^3 for the transition $nl \rightarrow n'l'$ can be written as

$$N^{v}_{nl,n'l'} = N^{O^{8+}} N^{H} v B_{nl,n'l'} \left(\sigma_{nl} + \sum_{n''>n} C_{n''l'',nl} \sigma_{n''l''} \right), \quad (9)$$

where $N^{O^{8+}}$ is the density of O^{8+} ions, N^{H} is the density of hydrogen atoms, v is the collision velocity, $C_{n''l'',nl}$ is the cascade matrix, and $B_{nl,n'l'}=A_{nl,n'l'}/\Sigma_{n''<n}A_{nl,n''l''}$. The radiative transition probabilities $A_{nl,n'l'}$ have been calculated by the wave functions of the Debye-Hückel potential. The spectral lines in plasmas can be broadened by the Doppler, Stark, and collisional mechanisms. Here, however, we shall neglect the specific details of the broadening and assume a Gaussian line profile with an arbitrary linewidth Γ. The reduced line intensity then can be defined as

$$I^{v}_{nl \rightarrow n'l'}(E_v) = [N^{v}_{nl \rightarrow n'l'}/(N^{O^{8+}} N^{H})] \frac{1}{\sqrt{2\pi}\Gamma} \exp\left[- \frac{(E_v - E_{v_0})^2}{\Gamma^2} \right], \quad (10)$$

where $E_{v_0}(=\Delta E_{nl,n'l'})$ is the transition energy.

From the decrease in energy differences of the O^{7+} bound states (having different principal quantum numbers) with decreasing the screening length (see, e.g., Fig. 2) it follows immediately that the spectral lines of O^{7+} ion, associated with the transitions $nl \rightarrow n', l \pm 1$ ($n' < n$), will be redshifted with respect to those of the unscreened case. Their redshift increases with decreasing r_d. However, the variation in line intensities with the screening will depend not only on the r_d variation in electron capture cross section for the particular upper nl state of the radiative transition but also on the r_d variation in capture cross sections to states higher than nl (contributing to the population of nl state via radiative cascading). As we have seen in Figs. 7 and 8, the nl-capture cross sections may have quite different energy behavior when r_d changes. This indicates that the variation in intensity of each specific spectral line for a given collision energy and screening length r_d can be quite different.

In Figs. 13(a) and 13(b) we show the reduced intensity of Ly-α line of O^{7+} produced by the electron capture process at collision energies of 0.5 and 5 keV/u, respectively, for the unscreened and screened cases with $r_d=12a_0$, $6a_0$, $4a_0$, and $2.5a_0$. As we have seen in Secs. I–III, the upper $2p$ state of this transition is not populated by a direct electron capture transition; its population is exclusively due to the cascades. The redshifts of the line at the collision energy of 0.5 keV/u for different values of r_d [Fig. 13(a)] do not show a distinct regularity for the reasons mentioned above. The intensity of the line for $r_d=12$ in Fig. 13(a) is larger than that for the unscreened case because at this energy the $5g$-partial cross section, which dominantly contributes to the population of $2p$ state trough the cascade path $5g$-$4f$-$3d$-$2p$, is larger than the $5g$ capture cross section in the unscreened case. The dif-

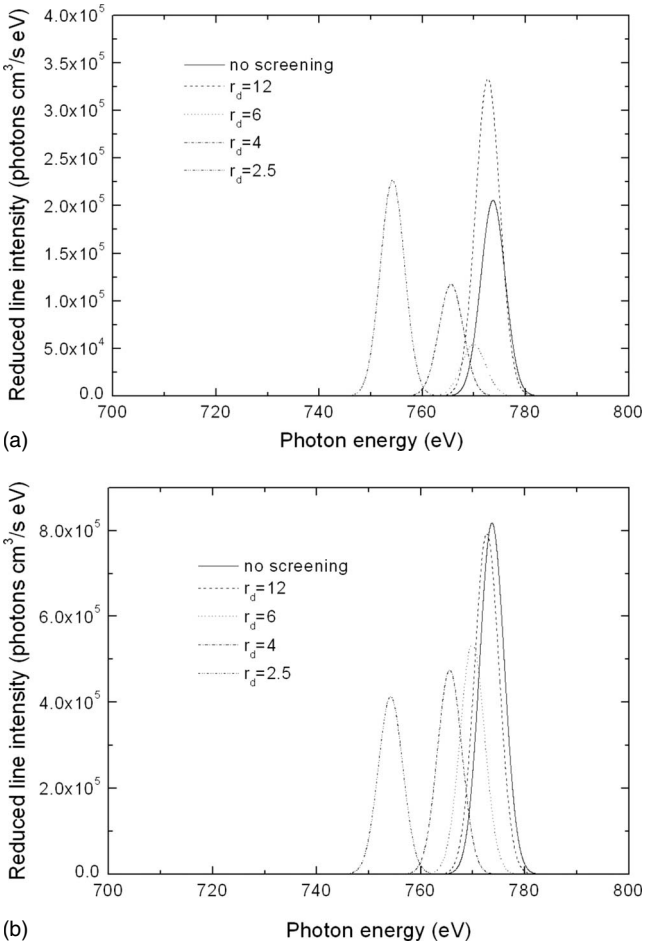

FIG. 14. Reduced intensity of Ly-β line of O^{7+} ion produced by electron capture at collision energies of (a) 0.5 and (b) 5 keV/u for the unscreened and screened cases with $r_d=12a_0$, $6a_0$, $4a_0$, and $2.5a_0$.

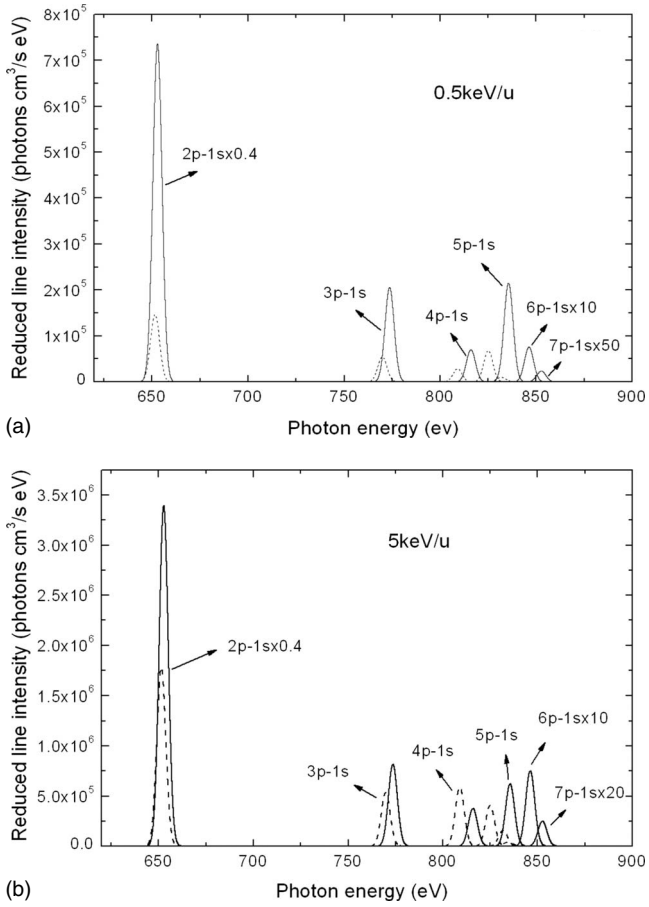

FIG. 15. Intensity of Lyman series line of O^{7+} produced by the electron capture process at collision energies of (a) 0.5 and (b) 5 keV/u for the unscreened (solid line) and screened case with $r_d=6a_0$ (dashed line).

ference of line intensities for $r_d=4a_0$ and $r_d=6a_0$ in Fig. 13(a) is due to the large difference in the $4f$ capture cross sections at $E=0.5$ keV/u (a factor of about 10) for these two screening lengths [see Figs. 7(b) and 7(c)]. The Ly-α intensity for $r_d=2.5a_0$ at this collision energy is also large because of the large capture cross section to the $3d$ state of O^{7+}.

For the collision energy of 5 keV/u, the shifts and intensities of Ly-α line show quite "regular" behavior: with decreasing r_d the line is increasingly more redshifted with respect to the unscreened interaction value and its intensity decreases. The Lyman-β line for these two energies and screening lengths shows the same behavior as the Lyman-α line (Fig. 14).

The fact that for a given value of the screening length the Debye-Hückel potential supports only a finite number of bound states implies that the spectral series of hydrogenlike systems contains a finite number of lines. The termination of Lyman series in a dense hot laser produced carbon plasma has recently been experimentally observed [28]. In Fig. 15 we show the lines of the Lyman series for $r_d=6a_0$ at the collision energies of 0.5 [panel (a)] and 5 keV/u [panel (b)], compared with the lines of this series in the unscreened case. As mentioned earlier, for $r_d=6a_0$ only the states with $n\leq 6$ and $7s$ and $7p$ states are in the discrete spectrum of O^{7+}. The relative intensity of different lines in the series reflects the electron capture population of the radiating state and all the states above involved in the corresponding cascade. It is to be noted that for these two energies and selected value of r_d the line intensity in the unscreened case is always larger than in the screened case, except for the $4p\rightarrow 1s$ line.

V. CONCLUSIONS

We have investigated the electron capture process in O^{8+}+H collisions in a Debye plasma by using the TC-AOCC method in the energy range of 0.2–50 keV/u. The AO expansion basis used in the present study included all the $n\leq 2$ states on H^+ and all the $n\leq 7$ states on O^{7+} (a total of 84 states) and was found to be fully convergent in the energy range considered in both the unscreened and screened cases (hence, it ensures the numerical reliability of obtained results).

The effects of the interaction screening that have the strongest influence on the electron capture dynamics in the O^{8+}+H collision system are the number of remaining bound states in the system for a given value of the screening length, the decrease in exchange couplings with decreasing r_d, and

the decrease of energy differences of the states with decreasing r_d. The last of these factors plays a major role at collision energies below 3–5 keV/u and causes some of the partial cross sections in the screened case to become larger than in the unscreened case. The effect of the decrease in energy differences of initial and capture states with decreasing r_d causes even the total cross section for the interaction screening with $r_d=12a_0$ to be larger than that of the unscreened case for energies below ~ 2 keV/u. As in the unscreened case, the dominant contribution to the total capture cross section in the considered energy range gives the $n=5$ partial cross section. However, while the $n=6$ cross section in the unscreened case becomes comparable with that for $n=5$ for energies below 0.5 keV/u, in the screened case the capture to $n=6$ is significantly suppressed.

In the present work we have also studied the properties of spectral lines associated with the radiative transitions of captured electrons in the Debye plasma. With respect to the unscreened case, the spectral lines are redshifted, but their intensities strongly depend on the collision energy at which the electron capture takes place, reflecting the energy dependence of nl-partial cross section for a given value of the screening length. Since in the considered collision system in the considered energy range the states within the $n=4,5,6$ manifolds are dominantly populated (when they are still in the discrete spectrum), the line intensities of the transitions between lower states are determined almost exclusively by the cascades populating the upper state of the considered transition. The reduction in the number of bound states in a screened Coulomb potential limits the spectral series to a finite number of lines for a given value of the screening length. Line shifts and series termination are important signatures that can be used in hot dense plasma diagnostics.

ACKNOWLEDGMENTS

One of us (R.K.J.) would like to express his gratitude to the Institute of Applied Physics and Computational Mathematics, Beijing, for the warm hospitality during the period when this work was performed. This work was partly supported by the National Natural Science Foundation of China (Grants No. 10875017, No. 10734140, No. 10844002, and No. 10604011) and the National Key Laboratory of Computational Physics Foundation (Grant No. 9140C6904030808).

[1] *Review of Fundamental Processes and Applications of Atoms and Ions*, edited by C. D. Lin (World Scientific, Singapore, 1993).
[2] *Atomic and Molecular Processes in Magnetic Fusion Edge Plasmas*, edited by R. K. Janev (Plenum, New York, 1995).
[3] *Handbook of Atomic, Molecular and Optical Physics, Part F: Application of Atomic and Molecular Physics to Astrophysics*, 2nd ed., edited by W. Drake (Springer, Berlin, 2006).
[4] R. K. Janev, L. P. Presnyakov, and V. P. Shevelko, *Physics of Highly Charged Ions* (Springer, Berlin, 1985).
[5] B. H. Bransden and M. R. C. McDowell, *Charge Exchange and the Theory of Ion-Atom Collisions* (Clarendon, Oxford, 1992).
[6] E. W. Mc Daniel, *Atomic Collisions: Heavy Particle Projectiles* (Willey, Toronto, 1993).
[7] J. C. Weisheit, Adv. At. Mol. Phys. **25**, 101 (1988).
[8] D. Salzman, *Atomic Physics in Hot Plasmas* (Oxford University Press, Oxford, 1998).
[9] M. S. Murillo and J. C. Weisheit, Phys. Rep. **302**, 1 (1998).
[10] M. S. Murillo, in *Atomic Processes in Plasmas*, AIP Conf. Proc. No. 381, edited by A. L. Osterheld and W. H. Goldstein (American Institute of Physics, New York, 1996), p. 231.
[11] C. G. Kim and Y. D. Jung, Phys. Plasmas **5**, 2806 (1998).
[12] N. Bohr and J. Lindhard, K. Dan. Vidensk. Selsk. Mat. Fys. Medd. **28**, 7 (1954).
[13] H. Zhang, J. G. Wang, B. He, Y. B. Qiu, and R. K. Janev, Phys. Plasmas **14**, 053505 (2007).
[14] S. L. Zeng, L. Liu, J. G. Wang, and R. K. Janev, J. Phys. B **41**, 135202 (2008).
[15] L. Liu, J. G. Wang, and R. K. Janev, Phys. Rev. A **77**, 032709 (2008).
[16] L. Liu, J. G. Wang, and R. K. Janev, Phys. Rev. A **77**, 042712 (2008).
[17] W. Fritsch and C. D. Lin, Phys. Rep. **202**, 1 (1991).
[18] W. Fritsch and C. D. Lin, Phys. Rev. A **29**, 3039 (1984).
[19] E. J. Shipsey, T. A. Green, and J. C. Browne, Phys. Rev. A **27**, 821 (1983).
[20] M. Kimura and N. F. Lane, Phys. Rev. A **35**, 70 (1987).
[21] M. Bendahman, S. Bliman, S. Douson *et al.*, J. Phys. (Paris) **46**, 561 (1985).
[22] T.-G. Lee, M. Hesse, A.-T. Le, and C. D. Lin, Phys. Rev. A **70**, 012702 (2004).
[23] J. Kuang and C. D. Lin, J. Phys. B **30**, 101 (1997).
[24] C. M. Reeves, J. Chem. Phys. **39**, 1 (1963).
[25] L. D. Landau and E. M. Lifshitz, *Quantum Mechanics: Non-Relativistic Theory* (Pergamon, London, 1958).
[26] F. W. Meyer, A. M. Howald, C. C. Havener, and R. A. Phaneuf, Phys. Rev. A **32**, 3310 (1985).
[27] K. Richter and E. A. Solov'ev, Phys. Rev. A **48**, 432 (1993).
[28] M. Nantel, G. Ma, S. Gu, C. Y. Côté, J. Itatani, and D. Umstadter, Phys. Rev. Lett. **80**, 4442 (1998).